Applied Catalysis B: Environmental 329 (2023) 122580

Contents lists available at ScienceDirect

Applied Catalysis B: Environmental

journal homepage: www.elsevier.com/locate/apcatb

Photocatalytic inactivation of airborne bacteria onto g-C_3N_4/TiO_2/Ni-polydopamine/Ni bifunctional coupling filter with non-size dependent capture effect

Linghui Peng [a,b], Haiyu Wang [a,b], Guiying Li [a,b], Weiping Zhang [a,b], Zhishu Liang [a,b], Taicheng An [a,b,*]

[a] Guangdong Key Laboratory of Environmental Catalysis and Health Risk Control, Guangdong-Hong Kong-Macao Joint Laboratory for Contaminants Exposure and Health, Institute of Environmental Health and Pollution Control, Guangdong University of Technology, Guangzhou 510006, China
[b] Guangdong Engineering Technology Research Center for Photocatalytic Technology Integration and Equipment, Guangzhou Key Laboratory of Environmental Catalysis and Pollution Control, School of Environmental Science and Engineering, Guangdong University of Technology, Guangzhou 510006, China

ARTICLE INFO

Keywords:
Bioaerosol
Bifunctional coupling filter
Non-size dependent capture
Photocatalytic inactivation
Inactivation mechanism

ABSTRACT

Most commercial air purifiers rely on dense fibrous filters for bioaerosols control, which filter the particulate matter size-dependently without bactericidal activity. Herein, the non-size-dependent bifunctional nickel foam filters (g-C_3N_4/TiO_2(CT)/Ni-polydopamine(PDA)/Ni bifunctional filter) with two layers of coupling nickel foams deposited by CT and PDA, respectively, were developed. The bifunctional filter shows remarkable non-size dependent bacteria removal efficiency (93.5 %) and inactivation efficiency (~70 %) within 20 min at high airflow (12.5 L min^{-1}). The inactivation efficiency can be further increased to 99.99 % with prolong irradiation time and enhancement of light intensity. The non-size dependent capture effect of the CT/Ni-PDA/Ni provided by adhesive force and charge was verified. In addition, the assumption that reactive oxygen species (ROSs) could be transferred into air during bacteria inactivation was first proved by chemiluminescent. This pioneered study may provide new insights into the development of bifunctional filters for non-size dependent capture and photocatalytic inactivation of bacteria in bioaerosols.

1. Introduction

Microorganisms in bioaerosols spread over long distances and remain alive for a long time, which may cause diseases, such as pneumonia, influenza, allergy and asthma if inhaled into the human body [1,2]. Recent outbreaks, including COVID-19, middle east respiratory syndrome (MERS), and severe acute respiratory syndrome (SARS), have been reported that posed by virus and pathogenic microorganisms in bioaerosols, which seriously threaten the global public health [3–6]. Therefore, it is of great significance to develop multiple functional materials for bioaerosols capture and complete inactivation of these biological contaminants.

Traditional capture methods of bioaerosols are size-dependent filtration, that is, the bioaerosols pass through small hole-size of filtration material and are passively intercepted [7–9]. The mechanisms of size-dependent filtration include inertial impact, direct interception, gravity settlement, Brownian diffusion and electrostatic interaction [10,11]. Based on the above filtration mechanisms, bioaerosols can be filtered by adjusting the pore size, specific surface area, porosity and surface charge of the porous material [12,13]. However, large pressure drop, easy blockage, low adhesive force and inability to inactivate bioaerosols are the major limitations of the filtration technology [14]. Biological contaminants in bioaerosols remain alive for a long time, and maybe accumulate and reproduce on the filter material, yielding secondary pollution [15–17]. Therefore, it is of great necessity to develop new multiple functional materials for non-size dependent capture with low pressure drop at high airflow rate and inactivation of biological contaminants in bioaerosols in situ [18,19].

Messersmith et al. first reported that dopamine molecules secreted by mussels can self-assemble and adhere onto any surfaces through intermolecular and intramolecular self-polymerization, forming polydopamine (PDA) membranes [20–22]. There are plenty of active groups

* Corresponding author at: Guangdong Key Laboratory of Environmental Catalysis and Health Risk Control, Guangdong-Hong Kong-Macao Joint Laboratory for Contaminants Exposure and Health, Institute of Environmental Health and Pollution Control, Guangdong University of Technology, Guangzhou 510006, China.
E-mail address: antc99@gdut.edu.cn (T. An).

https://doi.org/10.1016/j.apcatb.2023.122580
Received 19 July 2022; Received in revised form 3 January 2023; Accepted 4 March 2023
Available online 5 March 2023

on PDA membranes, which have an affinity to biological molecules, such as catechol group, phenolic hydroxyl group, amino group, aldehyde group, etc. PDA can form hydrogen bonds and chemical bonds with biological molecules [23]. Martín et al. have prepared core-shell Fe_3O_4 @poly(dopamine) magnetic nanoparticles for enabling many bio-molecules to be tightly immobilized onto their surfaces by covalent-linking [24]. Hu et al. reported a dopamine-modified hydrogel to adhere bio-tissues [25]. Therefore, PDA has potential applications in the "adhesive capture" of biological contaminants in bioaerosols.

On the other hand, photocatalytic technology shows great potential in inactivation of biological contaminants in bioaerosols due to its excellent oxidation capacity, environmental friendliness, no need for external equipment, good compatibility and so on [26–28]. Microorganisms such as bacterial cells can be attacked by reactive oxygen species (ROS) generated by photocatalysts and subsequently lead to cell death [26,29]. Jung and Forro et al. just loaded TiO_2 and photosensitive dyes on the surface of nanofibers to filter and pioneered the inactivation of bioaerosols under visible or ultraviolet light [30,31]. Wang et al. also designed photocatalytic metal organic framework (MOF) filters with 99.9999% inactivation efficiency of *E. coli* in bioaerosols within 2 h [32]. Sun et al. prepared two organic photosensitive composite membranes by electrospinning for filtering bioaerosols, reaching 99.9999 % inactivation of bacteria under daylight irradiation [33,34]. Bioaerosols are found to be filtered by the porous materials that modified by photocatalysts, achieving highly photocatalytic inactivation potential under various light irradiation. However, these biological contaminants may fall off, re-suspend in air and contaminate the loaded surfaces before inactivation due to the low adhesion strength between bioaerosols and the materials when it suffers airflow disturbance.

Therefore, the key challenge to solve the above problems is to develop a non-size-dependent bifunctional material not only with low pressure-drop and highly adhesive material but also with highly bactericidal activity to capture and continuously inactivate biological contaminants in bioaerosols at high airflow rates. In this study, a bifunctional filter, g-C_3N_4/TiO_2 (CT) and polydopamine (PDA) modified double-layer coupling nickel foam (CT/Ni-PDA/Ni bifunctional filter) was newly developed by incorporating the bioaerosols capture of PDA/Ni and the bacteria inactivation of CT/Ni. The relationships of the physical/chemical structures and airborne bacteria capture and inactivation performances of the CT/Ni-PDA/Ni bifunctional filter were revealed, illuminating the mechanisms of non-size dependent bioaerosols capture and photocatalytic inactivation. The double-layer CT/Ni-PDA/Ni bifunctional filter exhibits integrated advantages of high efficiency, low pressure-drop, long-term durability, and environmental friendliness, which may open a new avenue to develop a non-size-dependent bifunctional material for bioaerosols capture and inactivation at high airflow rates.

2. Experimental section

2.1. Preparation of CT/Ni-PDA/Ni bifunctional filter

The synthesis method of the g-C_3N_4/TiO_2 (CT) was described in our early published reference with a little modification [35] (See Supporting Information). The detailed preparation methods of the CT/Ni-PDA/Ni bifunctional filter were illustrated in the Supporting Information. Briefly, the washed Ni foams were immersed in the dopamine solution (namely PDA/Ni) and dried. We applied the electrophoresis technique to coat CT particles on conductive Ni foam to form CT/Ni, which is a quick and uniform coating method [36]. The other Ni foams were used as electrodes and applied voltage in CT water suspensions under stirring. After coating, the coated Ni foam was washed by pure running water and dried in a vacuum oven (denoted as CT/Ni). The CT/Ni was placed on the top of the PDA/Ni closely and the edges were compressed (called the CT/Ni-PDA/Ni) and sealed by O-ring in the quartz reactor with a hole in the middle.

2.2. Material characterization

The detailed material characterization was illustrated in the Supporting Information. Briefly, scanning electron microscopy (SEM) was performed on a Hitachi S-3400 N. Transmission electron microscopy (TEM) was carried out by a JEOL JEM-2100 microscope. Electron paramagnetic resonance (EPR) signals of spin-trapped paramagnetic species with DMPO (5,5-Dimethyl-1-pyrroline-N-oxide) were recorded with a Bruker A200 spectrometer. Fluorescence images of bacterial cells stained with Syto9 dye and PI dye were captured by Lionheart FX Automated Live Cell Imager with fluorescence microscopy (Biotek). Atomic force microscopy was carried out by a microscope (Dimension FastScan, Bruker). Electrophoresis was conducted by a DC power supply. Photocurrent measurements were performed in 0.5 M Na_2SO_4 solution by using a CHI 760E electrochemical workstation (Shanghai, China) with a standard three-electrode cell. The aerodynamic diameter of bioaerosol was measured by an Aerodynamic particle size spectrometer (TSI, APS 3321, America). The air pressure drops of the CT/Ni-PDA/Ni bifunctional filter, pure Ni and face mask were also measured by a digital differential pressure gauge.

2.3. Performance evaluation of CT/Ni-PDA/Ni bifunctional filter

2.3.1. Bioaerosols generation and balancing

Gram-negative *E. coli* (K-12) was used as model bacteria in bioaerosol in this work. The bacterial cells were cultivated in nutrient broth at 37 °C for 12 h to yield a cell count of approximately 10^9 CFU mL^{-1}. Then, the bacterial cells were collected by centrifugation (8000 rpm for 2 min) and resuspended in sterile saline solution (0.9 % (w/v)). Typically, 50 mL of bacteria solution (10^9 CFU mL^{-1}) was poured into glass bottle of BGI Collison bioaerosol generator. The bioaerosols capture and inactivation performances of the CT/Ni-PDA/Ni bifunctional filter were determined by using a self-built bioaerosols generation, balancing and inactivation system as shown in Fig. S1. Clean air with 12.5 L min^{-1} was injected into the generator and sprayed bioaerosols passed through the diffusion drying tube to control their relative humidity, and then went into the balancing chamber. The outlet of the system was connected with a pump and high-efficiency particulate air filter (HEPA) at the same flow rate, which makes air pressure balanced in the system. Before the experiment, the generated bioaerosols of *E. coli* were mixed and diluted in the 188 L Teflon balancing chamber with fan stirring. In order to avoid wall loss and settlement of bioaerosols, the filtration test was conducted through a continuous generation of bioaerosols with a steady concentration. The bioaerosol concentration was adjusted by the concentration of bacterial stock suspension (Fig. S2). After a continuous bioaerosols airflow rinsing of the whole system for 30 min, the CT/Ni-PDA/Ni filter was placed in the photocatalytic reactor (200 mL quartz reactor) with a 2 cm hole in diameter (Fig. S3) for filtration test.

2.3.2. Bioaerosols capture

Typically, the CT/Ni-PDA/Ni was placed in the quartz reactor with the layer of CT/Ni face to the Xenon lamp (0–400 mW cm^{-2}). The CT/Ni-PDA/Ni fully covered the hole to ensure the air flow go through the filter. After balancing for 30 min, the bioaerosols were filtered by the CT/Ni-PDA/Ni. The retention time of bioaerosols in the photocatalytic reactor was calculated as ~1 s and the face velocity was ~0.7 m/s (The calculation method is described in Supporting Information). The balancing concentration of living microorganisms in the balancing chamber was ~10^8 CFU m^{-3}. The filtered bioaerosols were collected by SKC biosampler (AGI-30) at the end of the airflow with 12.5 L min^{-1} for 20 min. The collected bacteria in the biosampler were diluted for plating and concentrated by CP-Select for fluorescence imaging (Innovaprep, America), followed by staining with dyes of LIVE/DEAD SytoYTO9/PI bacterial viability kit according to the manufacturer's protocol. The number of colonies was enumerated through visual inspection. The bacteria washed from the CT/Ni-PDA/Ni were collected and plating.

The comparison experiments of two layers of pure Ni were also conducted as the control experiment. All disks and materials were sterilized in an autoclave before experiments. The capture performance of the filter in dark under same conditions were also investigated.

2.3.3. Photocatalytic inactivation performance.

Firstly, the bioaerosols were filtered by the CT/Ni-PDA/Ni under illumination as mentioned above for 20 min. Then the PDA/Ni and the CT/Ni were separated and immersed into 20 mL 0.9 % (w/v) saline solutions under ultrasonic bath for 20 min, respectively. The solution was vortexed for 1 min and then diluted for plating. The concentrations of bacteria in eluant were determined by the standard plate count method. In order to better understand photocatalytic inactivation performance of the CT/Ni, we also conducted an individual experiment on each layer of the CT/Ni-PDA/Ni to demonstrate. The CT/Ni, PDA/Ni and pure Ni were exposed to a 12.5 L min^{-1} of aerosols flow for 2 min and then irradiated by visible light for 0–120 min at the density of 50–400 m Wcm^{-2}. After that, they were fully washed with 20 mL 0.9 % (w/v) saline solution in ultrasonic bath for 20 min. The concentrations of bacteria in eluant were determined by the standard plate count method. There were a series of experiments conducted in the dark at the same situations as the dark controls and the light control group was carried out with the CT/Ni, PDA/Ni, pure Ni and in the absence of the CT/Ni-PDA/Ni. All the experiments were repeated for three times.

2.4. ROS measurements

The photo-induced generation of $\bullet O_2^-$ and •OH were detected by the EPR technique using DMPO as the trapping agent in solution. For further verifying ROS generated and transmission in air, the Confocal Raman spectrometer (LabRAM HR Evolution) and chemiluminescent (CL) method were also employed. The CT/Ni layer of the CT/Ni-PDA/Ni was irradiated by UV (325 nm) laser for 5 min, and 50 μL luminol (100 μM) was dropped on the spot. Then the emission spectrum was recorded immediately. SOD was added into the luminol solution used as scavengers for $\bullet O_2^-$, and mannitol (100 mM, Aladdin, 99.5 %) was used for •OH (illustrated in Fig. S4). For ROS transmission measurement, the CT/Ni layer of the CT/Ni-PDA/Ni was placed on the top of a thin layer of luminol with a gap of ~1 mm under UV laser irradiation for 1 min, and then removed quickly, and the emission spectrum was recorded immediately, with 3 times repeated (illustrated in Fig. S5).

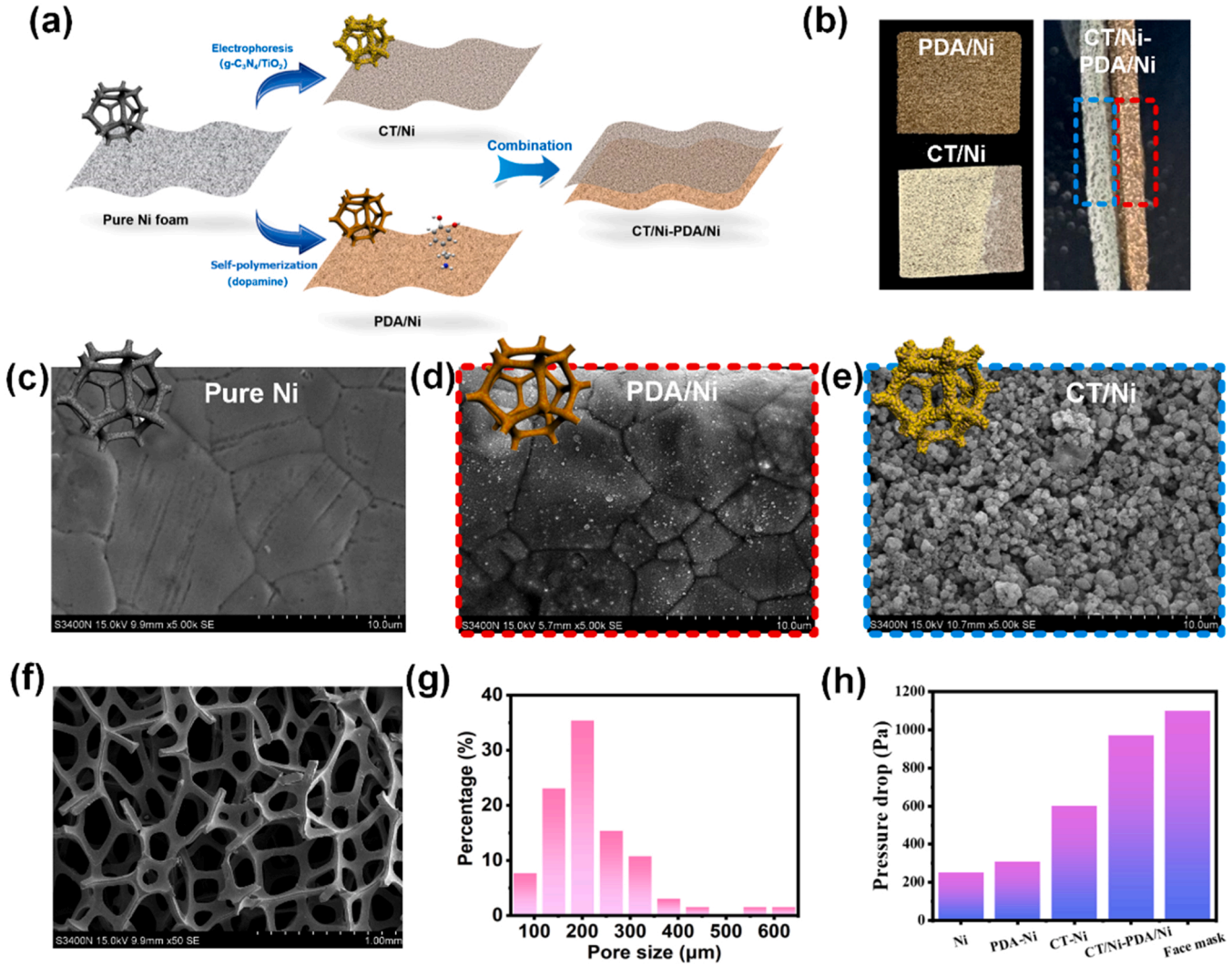

Fig. 1. Morphology and pressure drop of the CT/Ni-PDA/Ni. (a) Illustration of preparation procedure of the CT/Ni-PDA/Ni. SEM images of the porous Ni foam (b) at low magnification and (c) at high magnification. (d) The pore size distribution of the CT/Ni-PDA/Ni foam. (e) The comparison of pressure drops of the CT/Ni-PDA/Ni and other filters. (f) Digital images of the CT/Ni-PDA/Ni. SEM images of (g) the PDA modified and (h) the CT coating nickel foams of the CT/Ni-PDA/Ni at high magnification.

3. Results and discussions

3.1. Structure and composition analysis

The prepared CT/Ni-PDA/Ni bifunctional filter combines g-C_3N_4/TiO_2 loaded Ni foam (CT/Ni) and PDA modified Ni foam (PDA/Ni). As shown in Fig. 1a, two pieces of Ni foam were coated by CT nanoparticles by electrophoresis and PDA by self-assembly. The two layers of modified nickel foams were coupled together by compressing the edges of the nickel foam, forming the CT/Ni-PDA/Ni bifunctional filter. The optical photographs of the CT/Ni-PDA/Ni with front and side views were shown in Fig. 1b, showing a two-layer structure with light yellow and brown colors in appearance. The front view of the CT/Ni and PDA/Ni shows a significant color difference after treatment. It can be seen that the surface of the pure Ni foam is smooth with some grooves (Fig. 1c). Some small particles are formed on the surface of the PDA/Ni, but the grooves are still observed, indicating the PDA film is thin (Fig. 1d). The surface of the CT/Ni is fully uniformly covered by CT nanoparticles (characterized in Fig. S6-S8), no groove can be seen due to being fulfilled with nanoparticles (Fig. 1e). Element mapping shows that C, N, Ti and O elements are deposited on the Ni structure, indicating the successful preparation of the CT/Ni-PDA/Ni (Fig. S9). The CT/Ni-PDA/Ni is a porous structure with pore size of 100–600 μm and thickness of 50–100 μm of the skeleton structure (Fig. 1f). The pore size is majorly distributed at ~200 μm (Fig. 1g). Actually, the pore size of Ni foam is not influenced by surface modification of PDA and CT as shown in SEM images at lower magnification in Fig. S10. The aerodynamic diameter of *E. coli* bioaerosol is 1.54 μm and 1.33 μm at 80 % RH and 40 % RH, respectively (Fig. S11), indicating their penetration property. The aerodynamic diameter of *E. coli* bioaerosol is not influenced by the morphology, actual size and density of *E. coli*, but partly tells the size of the bacteria is much smaller than the pore size of the Ni foam. The results point to the fact that the CT/Ni-PDA/Ni doesn't reply on the small pore size (size sieving) of the filter for blocking bacteria but on a non-size dependent capture effect. As matter of fact, due to the fairly large pore size of the CT/Ni-PDA/Ni bifunctional filter, the pressure drop of it is relatively low, and even with 3 mm thickness shows lower pressure drop than that of the medical face mask (Fig. 1h). Indeed, the pressure drop of the CT/

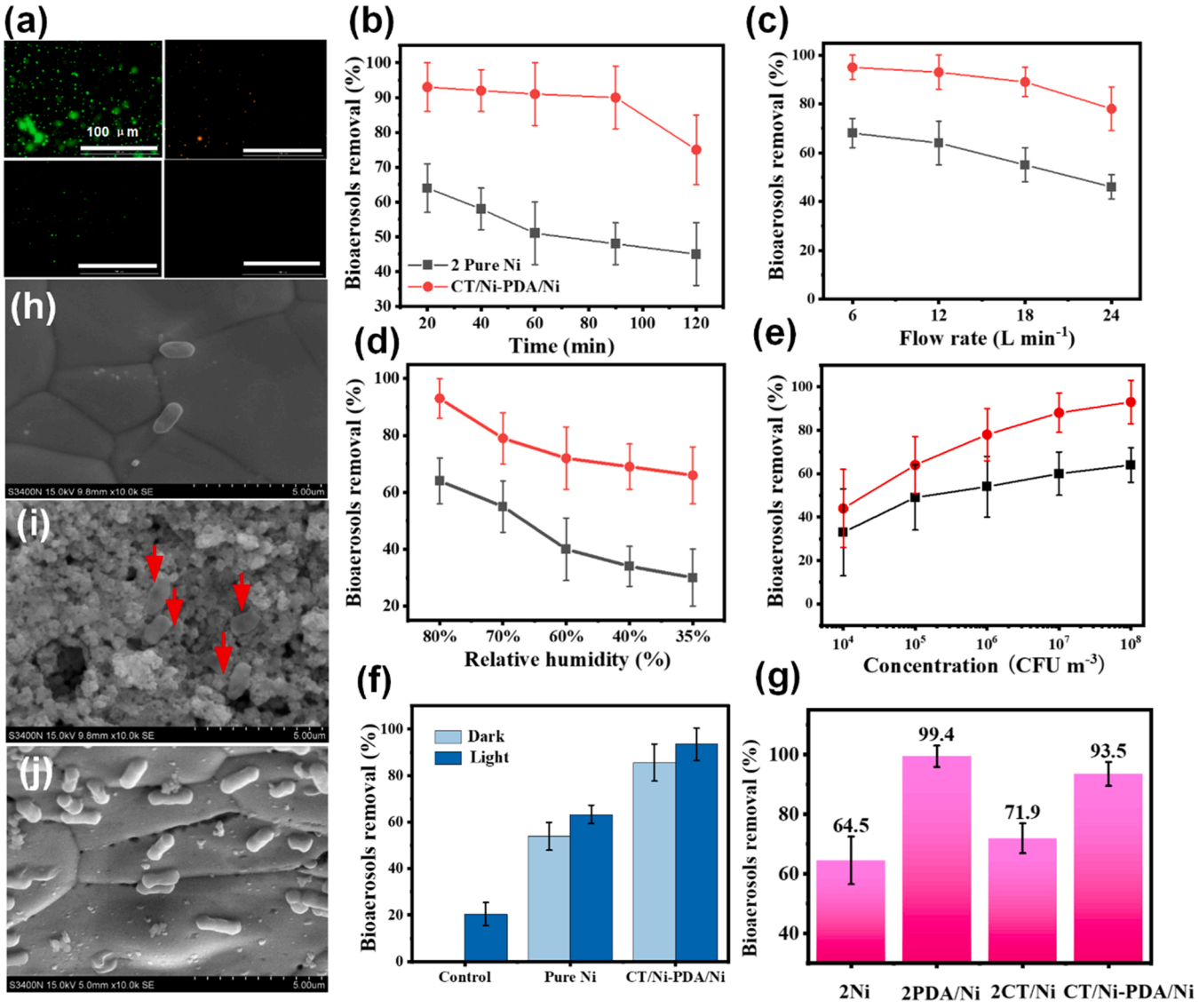

Fig. 2. Bioaerosols capture performance of the CT/Ni-PDA/Ni. (a) Fluorescent images of living and dead bacteria in bioaerosols before (top) and after (bottom) the CT/Ni-PDA/Ni filtration. Bioaerosols removal efficiencies of the CT/Ni-PDA/Ni and the 2 layers of the pure Ni at (b) different filtration time, (c) flow rate, (d) bioaerosol concentration, and (e) relative humidity. Comparisons of bioaerosols removal efficiencies of the CT/Ni-PDA/Ni (f) with and without light irradiation and (g) with the different filters. SEM images of the bacteria captured by (h) the pure Ni, (i) the CT/Ni and (j) the PDA/Ni.

Ni-PDA/Ni increased comparing with pure Ni due to surface modification on nickel skeletons. The surface roughness of Ni, the PDA/Ni layer and the CT/Ni layer of the CT/Ni-PDA/Ni are obtained as 62.3, 86.8 and 240.0 nm, respectively (Fig. S12). High surface roughness may contribute to the pressure drop due to air friction [37], leading to a higher pressure drop for the CT/Ni-PDA/Ni.

3.2. Bioaerosols capture performance of the bifunctional filter

The bioaerosols capture performance of the bifunctional filter was tested by filtering bioaerosols in our self-built bioaerosols generation, balancing and capturing system. The outlet bacteria in bioaerosols after filtering for 120 min by the CT/Ni-PDA/Ni bifunctional filter were collected by a biosampler and then concentrated for fluorescent imaging of living and dead cells. The top of Fig. 2a shows living (green) and dead (red) cells in the air before filtration by the CT/Ni-PDA/Ni bifunctional filter. Most of the bacteria are alive after long-distance transmission and fan balancing before filtration. In the bottom of Fig. 2a, the concentration of bacteria after filtering by the CT/Ni-PDA/Ni bifunctional filter is much lower than before, indicating significant bacteria removal efficiency of the CT/Ni-PDA/Ni. However, most of the bacteria in the air are still alive after the filtration. The results also show that if the bacteria in bioaerosols could not be captured by the CT/Ni-PDA/Ni bifunctional filter, they could not be inactivated, either. The bioaerosols removal efficiency of the CT/Ni-PDA/Ni bifunctional filter (~93.5 %) is ~40.0 % higher than the pure Ni foam filter (64.5 %) and is not significantly decreased after filtration for 120 min (Fig. 2c). Both the high flow rate and low relative humidity have negative impacts on the bioaerosols removal efficiency of the CT/Ni-PDA/Ni bifunctional filter and the pure Ni (Fig. 2c and d). The different air flow rates of filtration lead to different retention times and pressure drops, which may significantly influence the bioaerosols removal efficiency of the CT/Ni-PDA/Ni bifunctional filter. The removal efficiency of the CT/Ni-PDA/Ni bifunctional filter decreases from 93.5 % to 80.4 % when the flow rate ranges from 6 to 24 L min^{-1}. The higher flow rate leads to a short retention time of bioaerosols in the reactor, resulting in the greater shear force of airflow. The adhesion force of the CT/Ni-PDA/Ni bifunctional filter cannot capture the bacteria at too high airflow with a short retention time, yielding a poor removal efficiency of the bioaerosols. As we discussed the bioaerosols capture performance of the CT/Ni-PDA/Ni at different relative humidity, the aerodynamic diameter of *E. coli* bioaerosol at a dried environment is ~1 μm. The average aerodynamic diameter is 1.33 μm at 40 % RH. The smaller aerodynamic diameter of *E. coli* decreases the chance to contact with the surface of Ni foam, yielding lower capture efficiency. Interestingly, the bioaerosols removal efficiency of the CT/Ni-PDA/Ni bifunctional filter increases obviously with rise of the concentration of bioaerosols (Fig. 2e). The removal efficiency of the CT/Ni-PDA/Ni bifunctional filter increases from 42.7 % to 93.5 % when the bacterial concentration in air is increased from 10^4 to 10^8 CFU m^{-3}. Because the pore size of the CT/Ni-PDA/Ni bifunctional filter is much bigger than the size of bioaerosols, reducing the bacterial concentration will significantly decrease the probability of interaction between bioaerosols and Ni foam surface. The phenomenon mentioned above may be attributed to the interaction chances and the forces between the bacteria and the CT/Ni-PDA/Ni bifunctional filter, which will be discussed in the next part. All in all, the bifunctional filter performances outstanding bioaerosols capture efficiency with long service time at the high flow rate, high bacteria concentration, and relative humidity.

To make clear which part of the CT/Ni-PDA/Ni bifunctional filter enhances the capture performance, we compared the capture performance of the pure Ni, PDA/Ni, CT/Ni and CT/Ni-PDA/Ni. Blank control experiment shows that around 20 % of bioaerosols removal by light effect may be attributed to adhesion on walls, and inactivation by thermal effect and dehydration. Pure Ni filter shows only 60.3 % removal efficiency. However, the efficiency of the CT/Ni-PDA/Ni bifunctional filter is 93.5 % under light irradiation and keeps as high as 89.2 % in dark (Fig. 2 f), indicating that the bifunctional filter indeed improves the capture performance no matter with or without light irradiation. By comparing different combinations of the Ni foam with different modifications shown in Fig. 2 g, we found that PDA/Ni shows a significant higher bacteria removal efficiency than other samples. The removal efficiencies of the pure Ni and the CT/Ni are close at ~70 %, which indicates that the high removal efficiency of the CT/Ni-PDA/Ni bifunctional filter may come from the layer of PDA/Ni. We also prepared the CT/Ni-PDA/Ni bifunctional filter with different dopamine treatment times and concentrations to figure out if the PDA modification provides the non-size dependent capture effect for it. The bioaerosols removal efficiency of the CT/Ni-PDA/Ni bifunctional filter increases and reaches a plateau with increase of PDA treatment time and PDA concentration at 0.5 g L^{-1} and 24 h, respectively as shown in Fig. S13. Further increasing them will not increase the efficiency. SEM images of the PDA/Ni layer of the CT/Ni-PDA/Ni bifunctional filter with different dopamine concentrations are presented in Fig. S14. The PDA particles grow bigger with the concentration increases, while become aggregate together when the concentration is higher than 2 g L^{-1}. The aggregated PDA particles are loosely deposited on the surface of Ni, decreasing adhesive force for capturing bacteria. These results give evidence of the contribution of PDA for bacteria capture in bioaerosols. However, in order to balance time & materials saving and performance, the optimal dopamine concentration and treatment time of PDA modification is 0.5 g L^{-1} and 24 h, respectively. SEM images of bacteria captured by pure Ni and the CT/Ni-PDA/Ni are presented in Fig. 2h-j. Few bacteria on the surface of the pure Ni and CT/Ni, while many bacteria can be seen on PDA/Ni, in accordance with the results of the removal efficiency of the CT/Ni-PDA/Ni coming from the PDA/Ni. The above results show that the bioaerosols capture performance of the CT/Ni-PDA/Ni bifunctional filter is enhanced by non-size dependent capture effect based on PDA/Ni, which is desired for continuous capture of high bioaerosols concentration, relative humidity and flow rate.

3.3. Inactivation performance of bacteria in bioaerosols by bifunctional filter

The bioaerosols inactivation performance of the bifunctional filter was estimated by standard spread plating techniques. It has been found that if the bacteria in bioaerosols can't be captured by the bifunctional filter, they can't be inactivated in air, either. In order to know if the bacteria captured by the CT/Ni-PDA/Ni bifunctional filter were really inactivated, the bacteria on the CT/Ni-PDA/Ni bifunctional filter were eluted by 20 mL saline solutions under ultrasonic bath for 20 min. The inactivation efficiencies of the CT/Ni-PDA/Ni at different conditions were investigated. Obviously, the inactivation efficiency of the CT/Ni-PDA/Ni (84.5 %) is much higher than that of the pure Ni (62.0 %) at 50 mW cm^{-2} irradiation, and grows higher with the enhancement of the irradiation intensity (Fig. 3a). The bioaerosol flow rate has negative impacts on the inactivation efficiency of the CT/Ni-PDA/Ni due to short retention time (Fig. 3b). On the other hand, the relative humidity doesn't show significant influence on the inactivation efficiency of the CT/Ni-PDA/Ni (Fig. 3c), while the inactivation efficiency of the CT/Ni-PDA/Ni decreases with an increase of concentration of the bioaerosols (Fig. 3d). The high concentration of bioaerosols is not easily be inactivated because of more bacteria on the CT/Ni-PDA/Ni filter. We prepared the CT/Ni-PDA/Ni bifunctional filter with different CT loading weights to figure out the impacts of CT loading weights on the inactivation efficiency, shown in Fig. 3e. It is obvious that the inactivation efficiency increases with the rise of CT loading weights, showing positive impacts of CT particles on the inactivation efficiency of the CT/Ni-PDA/Ni. In Fig. 3f, the ~4×10^4 CFU cm^{-2} living bacteria captured by the CT/Ni-PDA/Ni bifunctional filter in dark and are inactivated to ~1×10^4 CFU cm^{-2} during 20 min filtration process under light irradiation. However, for pure Ni, living bacteria captured in dark (~3.1×10^4 CFU cm^{-2}) is

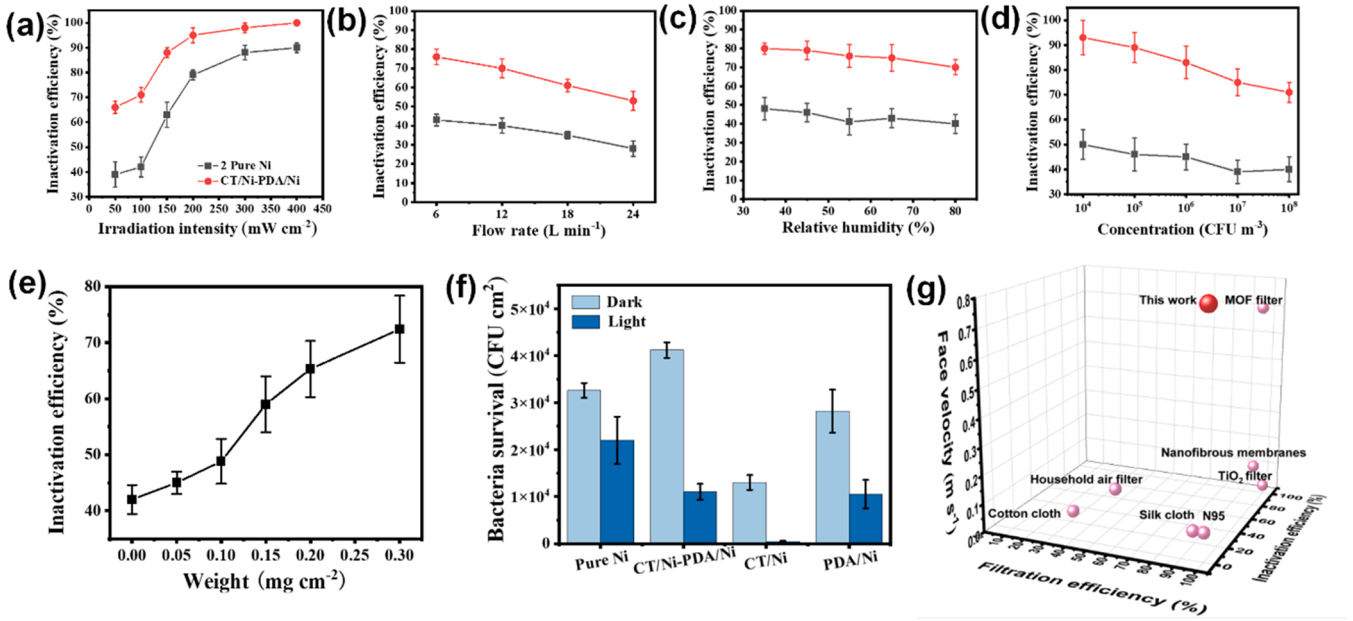

Fig. 3. Inactivation performance of bacteria in bioaerosols by CT/Ni-PDA/Ni. Bioaerosols inactivation efficiencies of the CT/Ni-PDA/Ni and the 2 layers of the pure Ni (a) at different irradiation intensity, (b) flow rate, (c) relative humidity, and (d) bioaerosol concentration. (e) Bioaerosols inactivation efficiency of the CT/Ni-PDA/Ni with different CT loading weight. (f) Bacteria survival on the CT/Ni-PDA/Ni with and without light irradiation. (g) Comparison of the CT/Ni-PDA/Ni and other filters.

less than that of the CT/Ni-PDA/Ni bifunctional filter, and only a few bacteria are killed under light (~2 $\times 10^4$ CFU cm^{-2}). The CT/Ni and PDA/Ni of the CT/Ni-PDA/Ni bifunctional filter were analyzed separately. We also found that for the CT/Ni layer, most of the bacteria on it are killed directly during the purification process under light, leaving only ~0.5 $\times$ 10^3 CFU cm^{-2} living bacteria. For the PDA/Ni layer, there are ~2.8 $\times$ 10^4 CFU cm^{-2} living bacteria on it before and only ~1 $\times$ 10^4 CFU cm^{-2} living bacteria after light irradiation. The survival bacteria on the CT/Ni-PDA/Ni and CT/Ni under light irradiation are remarkably reduced comparing with the pure Ni. On the other hand, the survival bacteria under light irradiation on the layer of PDA/Ni of the CT/Ni-PDA/Ni are less than that of the pure Ni, which may be attributed to the CT/Ni of the CT/Ni-PDA/Ni. Actually, the inactivation efficiency of the CT/Ni-PDA/Ni bifunctional filter increases with prolonged irradiation time, and the bacteria can be totally inactivated with additional light irradiation for 100 min (Fig. S15). The above results indicate that the CT/Ni offers the bacteria inactivation property to the CT/Ni-PDA/Ni bifunctional filter.

Comparisons of bioaerosols capture and inactivation efficiency between size-dependent and non-size dependent filters are also presented in Fig. 3g. Most of the size-dependent filters (or call fine filters) suffer from low face velocity and high pressure drop. Commercial household air filters show low bioaerosols removal efficiency and no bacterial inactivation, which may cause secondary contamination. Most studies of non-size dependent filtration based on electrostatic attraction, consuming a lot of energy for ultrafine particles [38] (See Table S1 for comparison). The CT/Ni-PDA/Ni bifunctional filter in this work shows high face velocity with fair bioaerosols capture and inactivation efficiency (highlighted by the red ball), which may show great potential for practical use in the future. In one word, the CT/Ni-PDA/Ni bifunctional filter is integrated with the two functions of non-size dependent capture and photocatalytic inactivation of bioaerosols.

3.4. *Bioaerosols capture and inactivation mechanisms onto the bifunctional filter*

The bioaerosols capture and inactivation mechanism of the bifunctional filter was investigated by measuring interaction forces and ROS generation/transmission of the filter. It is assumed that the bifunctions of bioaerosols capture and inactivation come from the top CT/Ni layer of the CT/Ni-PDA/Ni filter generates ROS transporting to downstream, while the bottom PDA/Ni layer of the CT/Ni-PDA/Ni captures the microorganisms in the air as shown in Fig. 4a. As mentioned above, the high bioaerosols removal efficiency of the CT/Ni-PDA/Ni comes from PDA/Ni, which is not dependent on the small pore size of the filter for blocking bacteria but on a non-size dependent capture effect. AFM was applied to detect the adhesion force on the PDA/Ni and CT/Ni surface of the CT/Ni-PDA/Ni bifunctional filter to reveal the bioaerosols capture mechanism of it. Fig. 4b shows that the adhesion force between the probe and the surface of PDA/Ni is 33.0 nN, which is 3 times higher than that of pure Ni (13.1 nN) and CT/Ni (11.2 nN). This strong adhesion force provided by PDA modification on the CT/Ni-PDA/Ni bifunctional filter can adhere the bacteria in bioaerosols and separate them from the bioaerosols flow. The adhesive force comes from the functional groups of the PDA, including phenolic hydroxyl group, aldehyde group, amino group and catechol group [20]. The characteristic peaks of functional groups of PDA/Ni are weak due to quite a thin PDA film on the Ni surface (Fig. 4c). In addition, the surface charge of the pure Ni and the PDA/Ni was also measured by AFM, which could be seen in Fig. 4d. The bigger deflection angle of the probe indicates the higher intensity of the surface charge. The charge distribution on the surface of the PDA/Ni is higher than that of pure Ni, which may attract bacteria that carry charges. The charges and adhesion forces of PDA come from its functional groups, leading to higher bioaerosols removal efficiency of the CT/Ni-PDA/Ni bifunctional filter.

As the bacteria survival on the CT/Ni-PDA/Ni bifunctional filter decreases significantly with increase of additional light irradiation after filtration, while for pure Ni control only drops a little, we assume that the bacteria are inactivated by the CT/Ni-PDA/Ni bifunctional filter based on photocatalytic mechanism. At the first stage, we suppose that the surface of the CT/Ni-PDA/Ni bifunctional filter is covered by a thin water film with bacteria at the first place, leading to photocatalytic ROS generation in water for inactivation [39,40]. Then, the bacteria are dried due to water evaporation at high air flow, yielding a fast bacteria inactivation efficiency at this stage by dehydration of bacteria and photocatalytic inactivation. After that, it is hypothesized that the ROSs

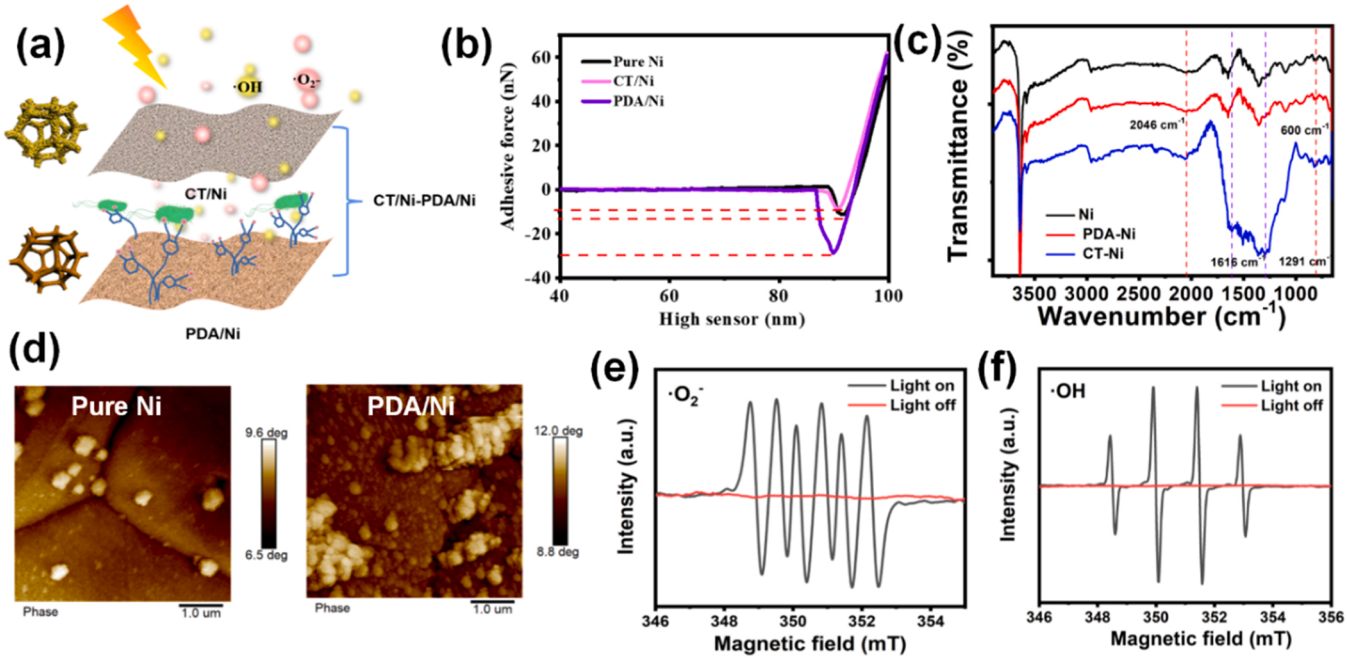

Fig. 4. Mechanism of the CT/Ni-PDA/Ni for bioaerosols capture and inactivation. (a) Illustration of the two functions of the CT/Ni-PDA/Ni filter. (b) Adhesive forces between the probe and the Ni with and without modification. (c) FTIR spectra of the CT/Ni-PDA/Ni. (d) Surface charge of the pure Ni and the PDA/Ni. EPR spectra of (e)·O_2^- and (f)·OH.

generate in air for bacteria inactivation. SEM image of *E. coli* cells on the CT/Ni after light irradiation, as indicated by the red arrows, shows that the morphology of the cells becomes irregular and cell membranes are broken (Fig. S16). The photocurrent response of pure Ni, and PDA/Ni & CT/Ni layers of the CT/Ni-PDA/Ni bifunctional filters indicates that the CT/Ni layer of the CT/Ni-PDA/Ni bifunctional filter plays the major photo-response for photocatalytic inactivation (Fig. S17). The EPR spectra of the DMPO-•O_2^- signal of the CT/Ni layer of the CT/Ni-PDA/Ni can be observed with light on, while no signal when light off (Fig. 4e). The DMPO-•OH signal of the CT/Ni can be observed in Fig. 4f when light on and disappears when light off. These EPR spectra confirm that the CT/Ni generates ROSs for inactivation bacteria in water under visible light irradiation. The conduction band (CB) of TiO_2 (−0.40 V) is more positive than the LUMO of g-C_3N_4 (−1.12 V), while the valence band (VB) of TiO_2 (+2.80 V) is lower than the HOMO of g-C_3N_4 (+1.57 V) [42,43]. The combination of g-C_3N_4 and TiO_2 broadens the spectral usage for photocatalytic reactions. These results confirm that the bacteria captured by the CT/Ni layer of the CT/Ni-PDA/Ni bifunctional filter can be inactivated by ROSs produced by CT particles under visible light irradiation. On the other hand, the bioaerosols inactivation performance of the CT/Ni-PDA/Ni bifunctional filter mainly attributes to photocatalytic property of the CT/Ni. Based on the results above, the CT/Ni-PDA/Ni bifunctional filter appears to demonstrate photocatalytic activity for bioaerosols inactivation under visible light irradiation.

Indeed, bacteria captured by the CT/Ni-PDA/Ni bifunctional filter can be inactivated directly if they are on the CT/Ni layer by generated ROSs, and they are also partly inactivated on the PDA/Ni layer without direct ROSs generation on the PDA/Ni. Thus, we hypothesize that the ROSs generated by the CT/Ni can be transferred along with the bioaerosol airflow to the downstream to inactivate the captured bacteria on the surface of the PDA/Ni within the CT/Ni-PDA/Ni bifunctional filter. To figure out what happened to the surface of the CT/Ni-PDA/Ni bifunctional filter in air, we applied Raman chemiluminescence (Raman-CL) test to record chemiluminescence emission spectra of luminol when reacts with ROS generated by the CT/Ni-PDA/Ni bifunctional filter under light irradiation, by using mannitol and SOD as the scavengers of •OH and •O_2^-, respectively [41]. As shown in Fig. 5a, a peak at ~500 nm in the CT/Ni-PDA/Ni bifunctional filter under light

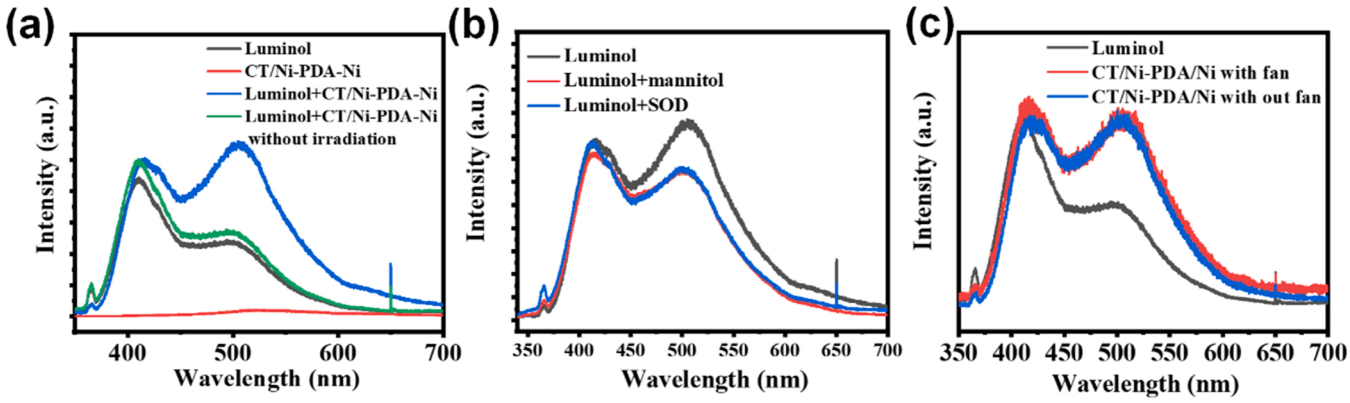

Fig. 5. ROS transmission for bioaerosols inactivation. (a) Raman emission spectra of (a) luminol with and without the CT/Ni-PDA/Ni and (b) the CT/Ni-PDA/Ni with luminol+SOD or mannitol for·O_2^- and·OH detection. (c) Raman emission spectra of the CT/Ni of the CT/Ni-PDA/Ni with and without a fan.

irradiation is obviously stronger than without light irradiation, indicating that ROS is truly generated in air. The emission spectra with and without SOD and mannitol in Fig. 5b indicate the existence of $\bullet O_2^-$ and •OH formed in air (weak due to quenching). For ROS transmission, we also used a fan to enhance the ROS transmission in air to react with luminol. It could be seen from Fig. 5c that the intensity of peak at 500 nm in CL emission spectra of luminol with the CT/Ni-PDA/Ni bifunctional filter on top (with and without a fan) is higher than that without it, indicating ROSs are transferred in air and react with luminol. These Raman-CL tests tell the evidences that ROSs generated on the surface of the CT/Ni layer of the CT/Ni-PDA/Ni bifunctional filter in air and can be transferred along with the air flow to the PDA/Ni layer for bacteria inactivation.

Therefore, the generated ROSs by CT/Ni not only inactivate bacteria on itself, but also can attack bacteria captured on the surface of the PDA/Ni layer within the CT/Ni-PDA/Ni bifunctional filter. The CT/Ni-PDA/Ni bifunctional filter exhibits high performance for bioaerosols non-size dependent capture as well as photocatalytic inactivation at high flow rate, bioaerosol concentration and relative humidity.

4. Conclusions

In summary, a non-size dependent CT/Ni-PDA/Ni bifunctional filter was explored for bioaerosols capture and photocatalytic inactivation for the first time. The bioaerosols removal efficiency of the CT/Ni-PDA/Ni bifunctional filter is ~93.5 % with 900 Pa pressure drop at a relatively high airflow rate of 12.5 L min^{-1} (face velocity of 0.7 m/s). It provides excellent bioaerosols removal performance at high concentration, flow rate and relative humidity of bioaerosols. The inactivation efficiency of the CT/Ni-PDA/Ni bifunctional filter reaches ~70% under visible light irradiation for 20 min, and over 99.99 % with additional irradiation for 100 min. It is found that the high removal efficiency of the CT/Ni-PDA/Ni bifunctional filter is enhanced by the PDA/Ni layer, while the photocatalytic inactivation function is offered by the CT/Ni layer and ROS transmission. The mechanism of the non-size dependent capture effect of the CT/Ni-PDA/Ni bifunctional filter is based on the adhesive force and charge attraction of the PDA. The photocatalytic inactivation effect of the CT/Ni-PDA/Ni bifunctional filter is attributed to ROSs generated on the surface of the CT/Ni layer of the CT/Ni-PDA/Ni, which can be transferred in air to attack bacteria on the surface of the PDA/Ni layer of the CT/Ni-PDA/Ni. The CT/Ni and the PDA/Ni are synergetically coupled, yielding two functions integrating within the CT/Ni-PDA/Ni bifunctional filter. This study shows that the CT/Ni-PDA/Ni bifunctional filter with non-size dependent capture effect possesses potential application of bioaerosols capture and photocatalytic inactivation with high efficiency and low pressure drop, which is necessary for public areas like hospitals, farms and plants.

CRediT authorship contribution statement

Linghui Peng: Methodology, Formal analysis, Writing – original draft. **Haiyu Wang:** Methodology, Data curation. **Guiying Li:** Writing – review & editing. **Weiping Zhang:** Visualization, Investigation. **Zhishu Liang:** Methodology, Validation. **Taicheng An:** Conceptualization, Supervision, Editing.

Declaration of Competing Interest

The authors declare that they have no known competing financial interests or personal relationships that could have appeared to influence the work reported in this paper.

Data availability

No data was used for the research described in the article.

Acknowledgements

This work was supported by National Natural Science Foundation of China (U1901210 and 42207112), Science and Technology Project of Guangdong Province, China (2021A0505030070 and 2022A1515010538), Local Innovative and Research Teams Project of Guangdong Pearl River Talents Program (2017BT01Z032), and China Postdoctoral Science Foundation Grant (2022M710822).

Appendix A. Supporting information

Supplementary data associated with this article can be found in the online version at doi:10.1016/j.apcatb.2023.122580.

References

[1] C. Humbal, S. Gautam, U. Trivedi, A review on recent progress in observations, and health effects of bioaerosols, Environ. Int. 118 (2018) 189–193.
[2] K.H. Kim, E. Kabir, S.A. Jahan, Airborne bioaerosols and their impact on human health, J. Environ. Sci. 67 (2018) 23–35.
[3] J.A. Lednickya, M. Lauzardo, Z.H. Fan, A. Jutla, T.B. Tilly, M. Gangwar, M. Usmani, S.N. Shankar, K. Mohanmed, A. Eiguren-Fernandez, C.J. Stephenson, M.M. Alam, M.A. Elbadry, J.C. Loeb, K. Subramaniam, T.B. Waltzek, K. Cherabuddi, J.G. Morris, C.Y. Wu, Viable SARS-CoV-2 in the air of a hospital room with COVID-19 patients, Int. J. Infect. Dis. 100 (2020) 476–482.
[4] L. Morawska, J. Cao, Airborne transmission of SARS-CoV-2: the world should face the reality, Environ. Int. 139 (2020), 105730.
[5] M. Yao, L. Zhang, J. Ma, L. Zhou, On airborne transmission and control of SARS-Cov-2, Sci. Total. Environ. 731 (2020), 139178.
[6] S. Herfst, M. Böhringer, B. Karo, P. Lawrence, N.S. Lewis, M.J. Mina, C.J. Russell, J. Steel, R.L. de Swart, C. Menge, Drivers of airborne human-to-human pathogen transmission, Curr. Opin. Virol. 22 (2017) 22–29.
[7] S.S. Zhou, S. Lukula, C. Chiossone, R.W. Nims, D.B. Suchmann, M.K. Ijaz, Assessment of a respiratory face mask for capturing air pollutants and pathogens including human influenza and rhinoviruses, J. Thorac. Dis. 10 (2018) 2059–2069.
[8] N.H. Leung, D.K. Chu, E.Y. Shiu, K.H. Chan, J.J. McDevitt, B.J.P. Hau, H.L. Yen, Y. G. Li, D.K.M. Ip, J.S.M. Peiris, W.H. Seto, G.M. Leung, D.K. Milton, B.J. Cowling, Respiratory virus shedding in exhaled breath and efficacy of face masks, Nat. Med. 26 (2020) 676–680.
[9] H. Souzandeh, K.S. Johnson, Y. Wang, K. Bhamidipaty, W.H. Zhong, Soy-protein-based nanofabrics for highly efficient and multifunctional air filtration, ACS Appl. Mater. Interfaces 8 (2016) 20023–20031.
[10] C.Y. Chen, Filtration of aerosols by fibrous media, Chem. Rev. 55 (1955) 595–623.
[11] G.Q. Gu, C.B. Han, C.X. Lu, C. He, T. Jiang, Z.L. Gao, C.J. Li, Z.L. Wang, Triboelectric nanogenerator enhanced nanofiber air filters for efficient particulate matter removal, ACS Nano 11 (2017) 6211–6217.
[12] C. Liu, P.C. Hsu, H.W. Lee, M. Ye, G.Y. Zheng, N.A. Liu, W.Y. Li, Y. Cui, Transparent air filter for high-efficiency $PM_{2.5}$ capture, Nat. Commun. 6 (2015) 1–9.
[13] X.W. Zhang, W. Zhang, M.Q. Yi, Y.J. Wang, P.J. Wang, J. Xu, F.L. Niu, F. Lin, High-performance inertial impaction filters for particulate matter removal, Sci. Rep. 8 (2018) 1–8.
[14] S. Zhang, H. Liu, X. Yin, J. Yu, B. Ding, Anti-deformed polyacrylonitrile/polysulfone composite membrane with binary structures for effective air filtration, ACS Appl. Mater. Interfaces 8 (2016) 8086–8095.
[15] J. Fröhlich-Nowoisky, C.J. Kampf, B. Weber, J.A. Huffman, C. Pöhlker, M. O. Andreae, N. Lang-Yona, S.M. Burrows, S.S. Gunthe, W. Elbert, H. Su, P. Hoor, E. Thines, T. Hoffmanm, V.R. Despres, U. Poschl, Bioaerosols in the earth system: climate, health, and ecosystem interactions, Atmos. Res.. 182 (2016) 346–376.
[16] W.W. Nazaroff, C.J. Weschler, Cleaning products and air fresheners: exposure to primary and secondary air pollutants, Atmos. Environ. 38 (2004) 2841–2865.
[17] M.T. Niu, F.X. Shen, F. Zhou, T.L. Zhu, Y.H. Zheng, Y. Yang, Y. Sun, X.H. Li, Y. Wu, P.Q. Fu, S. Tao, Indoor air filtration could lead to increased airborne endotoxin levels, Environ. Int. 142 (2020), 105878.
[18] L. Barbato, F. Bernardelli, G. Braga, M. Clementini, C. Di Gioia, C. Littarru, F. Oreglia, M. Raspini, E. Brambilla, I. Iavicoli, V. Pinchi, L. Landi, N.M. Sforza, R. Cavalcanti, A. Crea, F. Cairo, Surface disinfection and protective masks for SARS-CoV-2 and other respiratory viruses: a review by SIdP COVID-19 task force, Oral. Dis. 1 (2020) 1–9.
[19] Z. Zou, M. Yao, Airflow resistance and bio-filtering performance of carbon nanotube filters and current facepiece respirators, J. Aerosol. Sci. 79 (2015) 61–71.
[20] H. Lee, S.M. Dellatore, W.M. Miller, P.B. Messersmith, Mussel-inspired surface chemistry for multifunctional coatings, Science 318 (2007) 426–430.
[21] Q. Zhu, Q. Pan, Mussel-inspired direct immobilization of nanoparticles and application for oil-water separation, ACS Nano 8 (2014) 1402–1409.
[22] W. Cheng, X. Zeng, H. Chen, Z. Li, W. Zeng, L. Mei, Y. Zhao, Versatile polydopamine platforms: synthesis and promising applications for surface modification and advanced nanomedicine, ACS Nano 13 (2019) 8537–8565.
[23] B.K. Ahn, Perspectives on mussel-inspired wet adhesion, J. Am. Chem. Soc. 139 (2017) 10166–10171.
[24] M. Martín, P. Salazar, C. Jimenez, M. Lecuona, M.J. Ramos, J. Ode, J. Alcoba, R. Roche, R. Villalonga, S. Campuzano, J.M. Pingarron, J.L. Gonzalez-Mora, Rapid

Legionella pneumophila determination based on a disposable core-shell Fe_3O_4@poly(dopamine) magnetic nanoparticles immunoplatform, Anal. Chim. Acta 887 (2015) 51–58.
[25] C. Hu, L. Long, J. Cao, S. Zhang, Y. Wang, Dual-crosslinked mussel-inspired smart hydrogels with enhanced antibacterial and angiogenic properties for chronic infected diabetic wound treatment via pH-responsive quick cargo release, Chem. Eng. J. 411 (2021), 128564.
[26] O.K. Dalrymple, E. Stefanakos, M. A.Trotz, D.Y. Goswami, A review of the mechanisms and modeling of photocatalytic disinfection, Appl. Catal. B Environ. 98 (2010) 27–38.
[27] P. Murugesan, J.A. Moses, C. Anandharamakrishnan, Photocatalytic disinfection efficiency of 2D structure graphitic carbon nitride-based nanocomposites: a review, J. Mater. Sci. 54 (2019) 12206–12235.
[28] X.K. Zeng, Y. Liu, Y. Kang, Q.Y. Li, Y. Xia, Y.L. Zhu, H.L. Hou, M.H. Uddin, T. R. Gengenbach, D.H. Xia, C.H. Sun, D.T. Mccarthy, A. Deletic, J.G. Yu, X.W. Zhang, Simultaneously tuning charge separation and oxygen reduction pathway on graphitic carbon nitride by polyethylenimine for boosted photocatalytic hydrogen peroxide production, ACS Catal. 10 (2020) 3697–3706.
[29] B.C. Kim, E. Jeong, E. Kim, S.W. Hong, Bio-organic–inorganic hybrid photocatalyst, TiO_2 and glucose oxidase composite for enhancing antibacterial performance in aqueous environments, Appl. Catal. B Environ. 242 (2019) 194–201.
[30] E. Horváth, L. Rossi, C. Mercier, C. Lehmann, A. Sienkiewicz, L. Forró, Photocatalytic nanowires-based air filter: towards reusable protective masks, Adv. Funct. Mater. 30 (2020) 2004615.
[31] K.J. Heo, S.B. Jeong, J. Shin, G.B. Hwang, H.S. Ko, Y. Kim, D.Y. Choi, J.H. Jung, Water-repellent TiO_2-organic dye-based air filters for efficient visible-light-activated photochemical inactivation against bioaerosols, Nano Lett. 21 (2020) 1576–1583.
[32] P. Li, J.Z. Li, X. Feng, J. Li, Y.C. Hao, J.W. Zhang, H. Wang, A.X. Yin, J.W. Zhou, X. J. Ma, B. Wang, Metal-organic frameworks with photocatalytic bactericidal activity for integrated air cleaning, Nat. Commun. 10 (2019) 1–10.
[33] Y. Si, Z. Zhang, W.R. Wu, Q.X. Fu, K. Huang, N. Nitin, B. Ding, G. Sun, Daylight-driven rechargeable antibacterial and antiviral nanofibrous membranes for bioprotective applications, Sci. Adv. 4 (2018) eaar5931.
[34] P. Tang, Z. Zhang, A.Y. El-Moghazy, N. Wisuthiphaet, N. Nitin, G. Sun, Daylight-induced antibacterial and antiviral cotton cloth for offensive personal protection, ACS Appl. Mater. Interfaces 2 (2020) 49442–49451.
[35] G.Y. Li, X. Nie, J.Y. Chen, Q. Jiang, T.C. An, P.K. Wong, H.M. Zhang, H.J. Zhao, H. Yamashita, Enhanced visible-light-driven photocatalytic inactivation of Escherichia coli using g-C_3N_4-TiO_2 hybrid photocatalyst synthesized using a hydrothermal-calcination approach, Water. Res. 86 (2015) 17–24.
[36] A.H. Jayatissa, Electrophoresis coating of titanium dioxide nanoparticles in anodic nanotemplate, Proc. SPIE 5592 (2005) 400–405.
[37] S.G. Kandlikar, D. Schmitt, A.L. Carrano, J.B. Taylor, Characterization of surface roughness effects on pressure drop in single-phase flow in minichannels, Phys. Fluids 17 (2005), 100606.
[38] Y. Gao, E. Tian, J. Mo, Electrically responsive coarse filters endowed by high-dielectric-constant surface coatings toward efficient removal of ultrafine particles and ozone, ACS EST. Eng. 1 (2021) 1449–1459.
[39] T. Tatsuma, S.I. Tachibana, A. Fujishima, Remote oxidation of organic compounds by UV-irradiated TiO_2 via the gas phase, J. Phys. Chem. B 105 (2001) 6987–6992.
[40] K.I. Ishibashi, A. Fujishima, T. Watanabe, K. Hashimoto, Generation and deactivation processes of superoxide formed on TiO_2 film illuminated by very weak uv light in air or water, J. Phys. Chem. B 104 (2000) 4934–4938.
[41] S. Dong, H.M. Hwang, X. Shi, L. Holloway, H. Yu, UVA-induced DNA single-strand cleavage by 1-hydroxypyrene and formation of covalent adducts between DNA and 1-hydroxypyrene, Chem. Res. Toxicol. 13 (2000) 585.
[42] J. Yu, S. Wang, J. Low, W. Xiao, Enhanced photocatalytic performance of direct Z-scheme g-C_3N_4-TiO_2 photocatalysts for the decomposition of formaldehyde in air. Phys. Chem. Chem. Phys. 15 (2013) 16883–16890.
[43] N. Boonprakob, N. Wetchakun, S. Phanichphant, D. Waxler, P. Sherrell, A. Nattestad, J. Chen, B. Inceesungvorn, Enhanced visible-light photocatalytic activity of g-C_3N_4-TiO_2 films, J. Colloid. Interface 417 (2014) 402–409.